IAGI Journal
Volume 1 No. 3, December 2021: 121–136 *e*-ISSN 2776-0111

Pre-1963 Mount Agung Eruption History and Magma Evolution Based on Petrological, Mineralogical, and Geochemical Analyses

Aulia Syafitri[1]*, I Gusti Bagus Eddy Sucipta[2], Adzkia Noerma Arifa[1], Asep Saepuloh[2], Sri Widiyantoro[3,4]
[1]Laboratory of SEM-EDS UPP Chevron-Bandung Institute of Technology
[2]Petrology, Volcanology, and Geochemistry Research Group, Geological Engineering, Faculty of Earth Science and Technology-Bandung Institute of Technology
[3]Global Geophysics Research Group, Faculty of Mining and Petroleum Engineering-Bandung Institute of Technology
Ganesa St., No.10 Kota Bandung, Jawa Barat 40132, Indonesia
[4]Faculty of Engineering, Maranatha Christian University
Surya Sumantri St. No.65, Kota Bandung, Jawa Barat 40164, Indonesia
*E-mail: mauliasyafitri10@gmail.com

Article received: 23 November 2021, revised: 23 December 2021, accepted: 31 December 2021
DOI: 10.51835/iagij.2021.1.3.375

ABSTRACT

Mount Agung is an active stratovolcano on Bali Island. The eruption of Mount Agung, which took place in 1963, was the largest eruption after Mount Krakatoa in 1883 and became one of the most prominent eruptions in the 20th century. Pre-eruption history of Mount Agung has yet to be known in detail. This study aims to determine the history of the pre-1963 volcanic activity of Mount Agung. Based on statistical, petrological, and mineralogical data analyses, the result shows that the pre-1963 eruption of Mount Agung was influenced by three cogenetic magmas that can be divided into four eruption periods, i.e., pre-3200 ± 60 BP, 3200 ± 60 – 1870 ± 40 BP, 1870 ± 40 – 1040 ± 50 BP, and post-1040 ± 50 BP. Mount Agung's historical activity was marked by the injection of the basaltic magma in the pre-3200 ± 60 BP period and reached its peak in the 3200 ± 60 – 1870 ± 40 BP period. Both periods produced dominant basalt to basaltic andesite lava units (SiO2 51 – 56%). The end of the 3200 ± 60 – 1870 ± 40 BP period was marked by Bukit Pawon parasitic cone formation. In 1870 ± 40 – 1040 ± 50 BP, many pyroclastic flow units were formed in addition to the emergence of basalt to andesite lava units. During this period, magma differentiation continued as indicated by the rising content of SiO2 (51 – 58%), which was controlled by crystallization fractionation. During this period, a small injection of basaltic magma occurred, which caused the magma to mix with the previously differentiated magma. At the beginning of the post-1040 ± 50 BP period, there was a slight injection of basaltic magma. Afterward, magma underwent intensive differentiation coinciding with the increase of SiO2 (53 – 63%), followed by crystal fractionation and slight crustal contamination. The evolved magma can produce pyroclastic fall, pyroclastics flow, and lava units.

Keywords: Mount Agung, eruption periods, magma differentiation.

INTRODUCTION

Only 69 out of 120 volcanoes in Indonesia are monitored by the Centre of Volcanology and Geological Hazard Mitigation (PVMBG). Apart from the highest number of volcanoes, the number of victims due to volcanic disasters is also ranked first globally [1]. The condition suggests that the study of volcano and disaster mitigation in Indonesia has become essential. One of the critical pieces of information needed in volcanic hazard assessment is detailed historical records of volcanic activity [2].

Mount Agung is an active stratovolcano located in Karangasem Regency, eastern Bali Province. The eruption of Mount Agung in 1963 was the largest eruption with the highest magnitude in Indonesia, after Mount Krakatoa in 1883, and became one of the most predominant events in the 20th century due to its influence on the global climate [3,4]. This eruption released lahars, pyroclastic flows, lava, and volcanic earthquakes, which caused more than 2000 deaths [4–7].

Previous research on Mount Agung mainly focused on the 1963 eruption [3,4]. However, the pre-existing volcanic activity is not well recorded [2,4]. Information has mainly been gathered from the Balinese historical records, which mention eruptions in the 16th to 18th centuries, precisely in 1843, 1821, 1808, and 1711 [2]. Therefore, this study includes the comprehensive historical activity of Mount Agung, especially before 1963.

Mount Agung has one main crater at 3014 meters above sea level. In addition, Mount Agung also has a parasitic cone, Bukit Pawon, on the southeast slope with an altitude of 800 meters above sea level. The pre-1963 volcanic deposits consist of 14-lava units, 5-flow pyroclastic units, and 2-fall pyroclastic units [8]. Based on the volcano-stratigraphy (Figure 1), Mount Agung produced dominant lava units in the older period. Pyroclastic flow units began to appear in 1870 ± 40 BP, and pyroclastic fall units began to form in 1040 ± 40 BP.

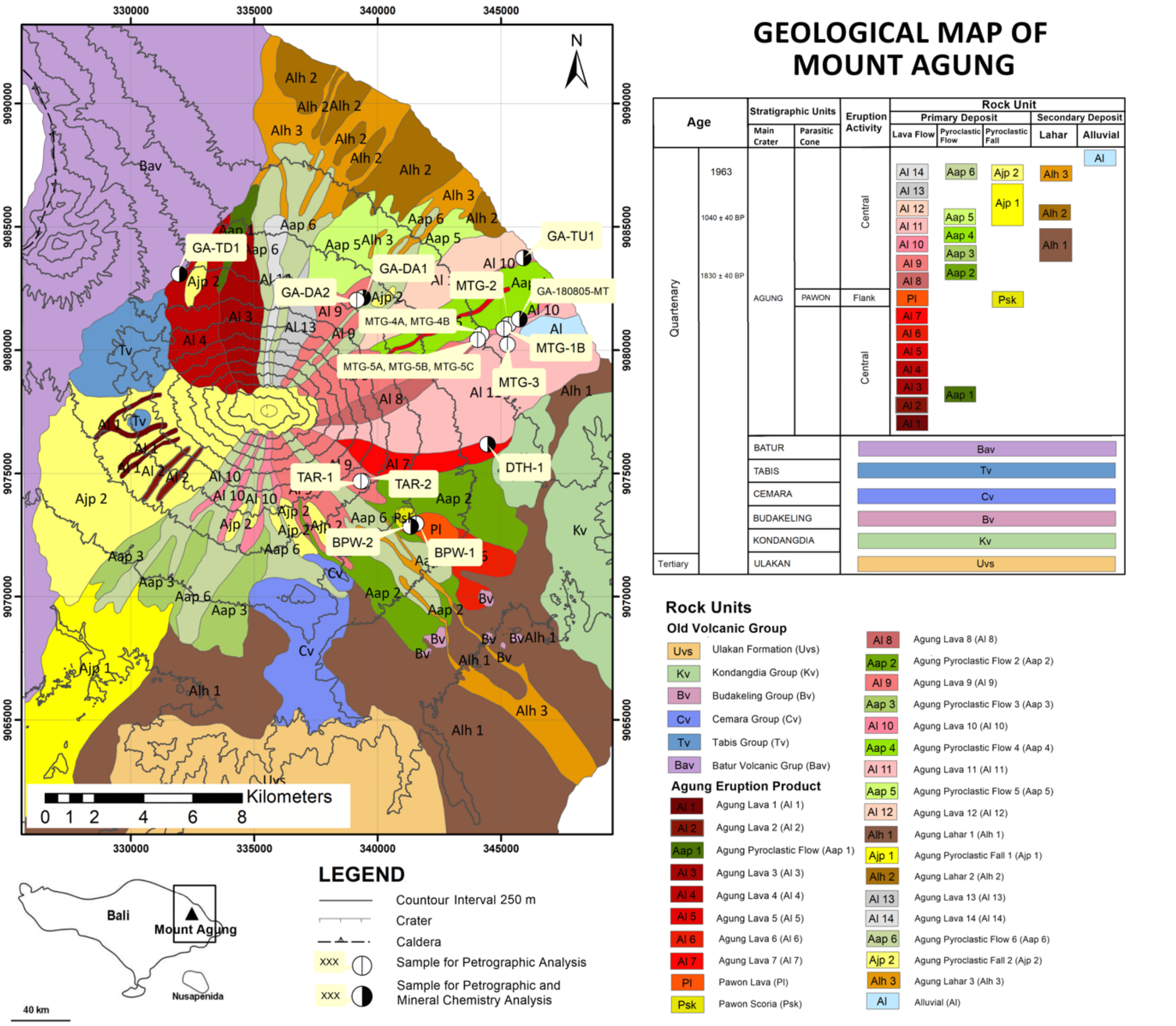

Figure 1. Geological map of Mount Agung [8]. The map is equipped with the sample location, consisting of 18 lava samples for petrography and six (6) samples for mineral chemistry analysis

METHODOLOGY

Well-preserved lava samples were taken from 18 outcrop locations around Mount Agung (Figure 1). Microscopy observations have been conducted using a polarizing microscope on all lava samples to observe the mineral composition. The geochemical analysis has been performed from the six selected samples using Scanning Electron Microscopy-Energy Dispersive X-Ray Spectrometry (SEM-EDS). The instrument used is JEOL JSM-IT-300 for SEM-EDS, carried out in the Laboratory of Chevron-Bandung Insitute of Technology, Indonesia. The test aimed to identify the major and minor element content (such as Ti, Al, Fe, Mn, Mg, Ca, Na, K, P, Cr, Ni) of the phenocrysts in the samples.

In addition, bulk geochemical analysis was obtained using additional published data from Fontjin's [2] (46 samples) and Dempsey's [9] (18 samples). The collected data from the literature consists of several major elements (SiO2, Al2O3, Fe2O3, FeO, MnO, MgO, CaO, Na2O, K2O, TiO2, P2O5) and trace elements (Rb, Sr, Y, Nb, Zr, Cr, Ni, Cu, Zn, Ga, Ba, Pb, Th, U, La, Ce, Nd, Sm). All of the sample used in this study is presented in Table 1.

Table 1. The list of samples used in this research includes 18 samples as primary data and 64 samples as supplementary data consisting of 46 samples from Fontijin [2] and 18 samples from Dempsey [9]

No.	Sample Code	Deposit Type	Thin Section (Petrographic Analysis)	SEM-EDS (Mineral Chemistry Analysis)	Reference : Fontjin et al. (2015)								Reference : Dempsey (2013)			
					No.	Sample Code	Deposit Type	ICP-OES, ICP-MS (Geochemical Analysis)	No.	Sample Code	Deposit Type	ICP-OES, ICP-MS (Geomichal Analysis)	No.	Sample Code	Deposit Type	ICP-MS, XRF (Geochemical Analysis)
1	**GA-TU1**	Lava	✓	✓	1	**AG008B**	Pumice	✓	24	**AG006bisF**	Ash Fall	✓	1	**Agu16**	Lava	✓
2	**MTG-3**	Lava	✓		2	**AG016C**	Scoria	✓	25	**AG006bisH**	Ash Fall	✓	2	**Agu18**	Lava	✓
3	**GA-180805-MT**	Lava	✓	✓	3	**AG012E**	Pyroclastic Flow	✓	26	**AG021C**	Scoria	✓	3	**Agu20**	Lava	✓
4	**MTG-1B**	Lava	✓		4	**AG028B**	Pyroclastic Flow	✓	27	**AG021D**	Ash Fall	✓	4	**Agu21**	Lava	✓
5	**MTG-2**	Lava	✓		5	**AG042B**	Pyroclastic Flow	✓	28	**AG021E**	Scoria	✓	5	**Agu22**	Lava	✓
6	**MTG-4A**	Lava	✓		6	**AG001bisH**	Pumice	✓	29	**AG021H**	Ash Fall	✓	6	**Agu23**	Lava	✓
7	**MTG-4B**	Lava	✓		7	**AG045D**	Pyroclastic Flow	✓	30	**AG021I**	Scoria	✓	7	**Agu24**	Lava	✓
8	**MTG-5A**	Lava	✓		8	**AG042D**	Pyroclastic Flow	✓	31	**AG021K**	Scoria	✓	8	**Agu25**	Pyroclastic	✓
9	**MTG-5B**	Lava	✓		9	**AG001bisB**	Pyroclastic Flow	✓	32	**AG006bisO**	Scoria	✓	9	**Agu06**	Pyroclastic	✓
10	**MTG-5C**	Lava	✓		10	**AG042G**	Pumice	✓	33	**AG006bisS**	Scoria	✓	10	**Agu07**	Pyroclastic	✓
11	**TAR-1**	Lava	✓		11	**AG001bisC**	Scoria	✓	34	**AG006bisR**	Ash Fall	✓	11	**Agu10**	Lava	✓
12	**TAR-2**	Lava	✓		12	**AG001bisE**	Pyroclastic Flow	✓	35	**AG006bisT**	Scoria	✓	12	**Agu12**	Lava	✓
13	**GA-DA1**	Lava	✓	✓	13	**AG042I**	Pyroclastic Flow	✓	36	**AG006bisK**	Scoria	✓	13	**Agu13**	Lava	✓
14	**GA-DA2**	Lava	✓		14	**AG042bisD**	Pyroclastic Flow	✓	37	**AG006M**	Scoria	✓	14	**Agu15**	Lava	✓
15	**BPW-1**	Lava	✓		15	**AG042bisB**	Pyroclastic Flow	✓	38	**AG006N**	Scoria	✓	15	**Agu03**	Pyroclastic	✓
16	**BPW-2**	Lava	✓	✓	16	**AG024E**	Pyroclastic Flow	✓	39	**AG006O**	Ash Fall	✓	16	**Agu30**	Lava	✓
17	**DTH-1**	Lava	✓	✓	17	**AG024D**	Pyroclastic Flow	✓	40	**AG006R**	Scoria	✓	17	**Agu31**	Lava	✓
18	**GA-TD1**	Lava	✓	✓	18	**AG008G**	Ash Fall	✓	41	**AG006S**	Scoria	✓	18	**Agu33**	Lava	✓
					19	**AG021L**	Ash Fall	✓	42	**AG021B**	Ash Fall	✓				
					20	**AG008I**	Scoria	✓	43	**AG006bisAB**	Scoria	✓				
					21	**AG008L**	Scoria	✓	44	**AG006B**	Scoria	✓				
					22	**AG006bisC**	Scoria	✓	45	**AG006F**	Scoria	✓				
					23	**AG006bisE**	Scoria	✓	46	**AG024B**	Pyroclastic Flow	✓				

RESULTS

Data and stratigraphic correlation were needed to find the relationship between the existing samples used in this research for better understanding. The correlation is based on: (1) the same absolute age in Nasution's geological map [8] and Fontjin's research [2] (Figure 2); (2) SiO_2 vs. K_2O diagram, which shows the existence of three cogenetic magma-differentiation (Figure 3). With those basics, the authors divided the pre-1963 Mount Agung volcanic activity into 4-periods, namely the post-1040 ± 50 BP, 1870 ± 40 BP – 1040 ± 50 BP, 3200 ± 60 BP – 1870 ± 40 BP, and the pre-3200 ± 60 BP period.

Petrography and Mineral Composition

Based on microscopic observations of 18 lava samples, all eruption periods produced pyroxene-andesite rocks (classified from [10]), which have a porphyritic texture. The phenocrysts composition is dominated by plagioclase, followed by pyroxene, opaque minerals, and olivine.

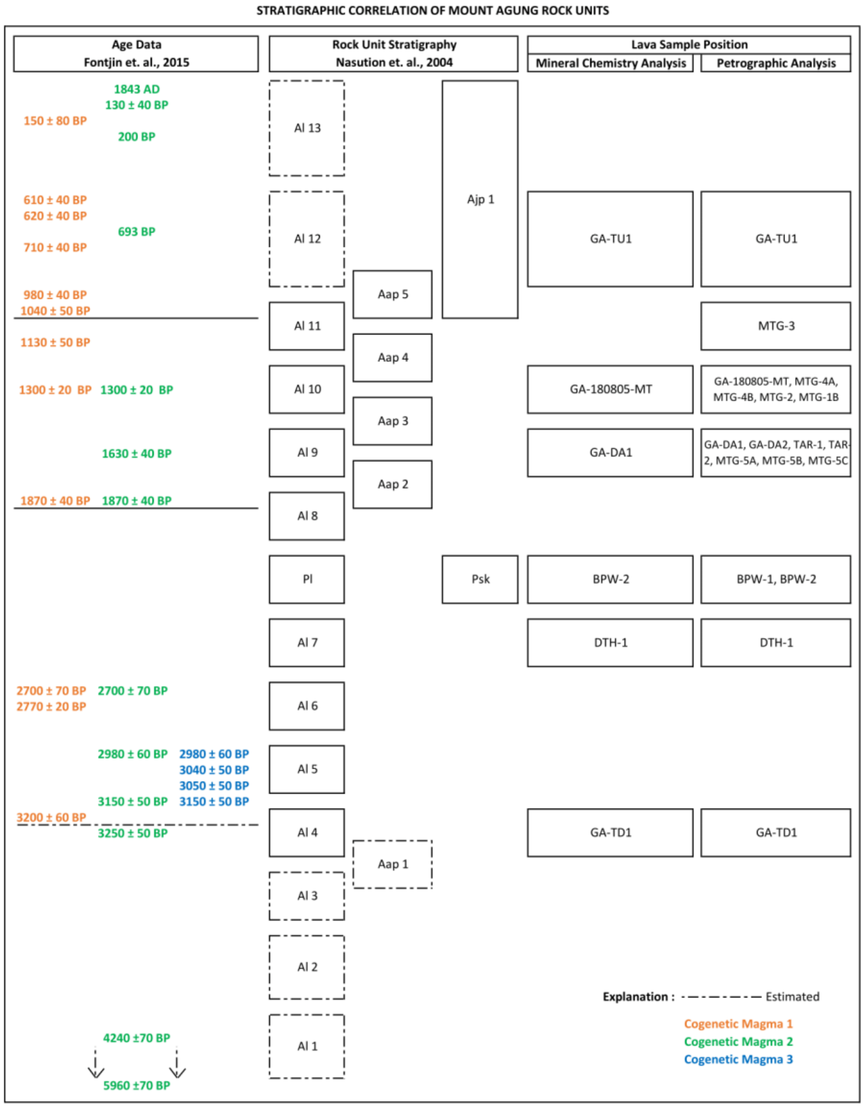

Figure 2. Data and stratigraphic correlation of age [2], rock units [8], and sample used in this study represent the rock units

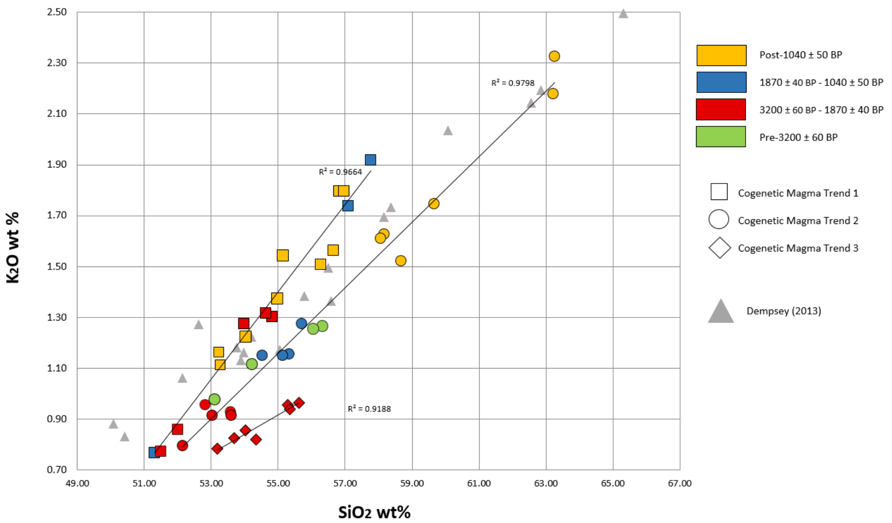

Figure 3. SiO2 against K2O diagram. The diagram shows three cogenetic magma trendlines and the distribution of the samples in each period. The used data are from [2]. Data from Dempsey [9] is presented as a comparison

IAGI Journal
Volume 1 No. 3, December 2021: 121–136 *e*-ISSN 2776-0111

Plagioclase is the predominant phenocryst presented in all samples. The crystal exhibits subhedral, varying microtextures (Figure 4). Coarse sieve is abundant, followed by glomerocryst, fine sieve, fine-oscillatory zoning, and resorption surface. Based on the An composition taken from mineral chemistry analysis (Figure 5), in pre-3200 ± 60 BP period, plagioclase contains a long-range of An38–89. The core tends to be more calcic than the rim. In the 3200 ± 60 – 1870 ± 40 BP period, the An content decreased to An67–83. Both core and rim have a wide range of An. In 1870 ± 40 – 1040 ± 50 BP, the An composition decreased to An43–88. In the post-1040 ± 50 BP period, plagioclase minerals have An38–86, with the same distribution pattern as the first period. The core is more calcic than the rim. According to the scanline test, the mass percentage of Ca in plagioclase decreased from the core to the rim in each eruption period (Figure 5).

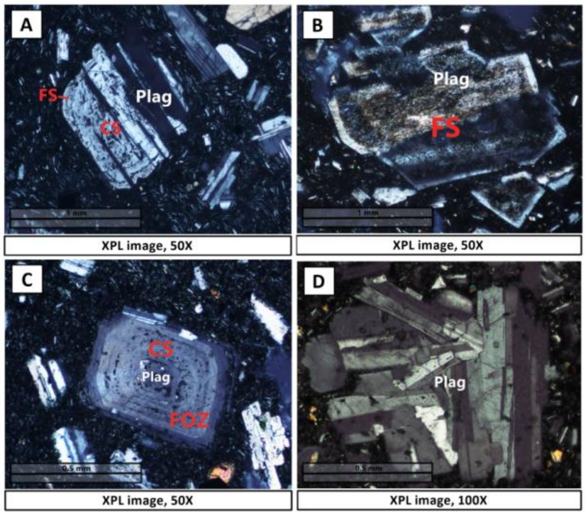

Figure 4. Selected images of the pre-1963 Mount Agung eruption products are presented in the form of plagioclase under the optical microscope observation. (A) Coarse sieve texture in Sample GA-TD1 (pre-3200 ± 60 BP). (B) Fine sieve texture found in Sample BPW-2 (3200 ± 60 – 1870 ± 40 BP). (C) Fine oscillatory zoning and coarse sieve texture in Sample TAR-2 (1870 ± 40 – 1040 ± 50 BP). (D) Glomerocryst texture in GA-TU1 (post-1040 ± 50 BP). In detail, the annotation includes Plag = Plagioclase; FS = Fine Sieve; CS = Coarse Sieve; FOZ = Fine Oscillatory Zoning

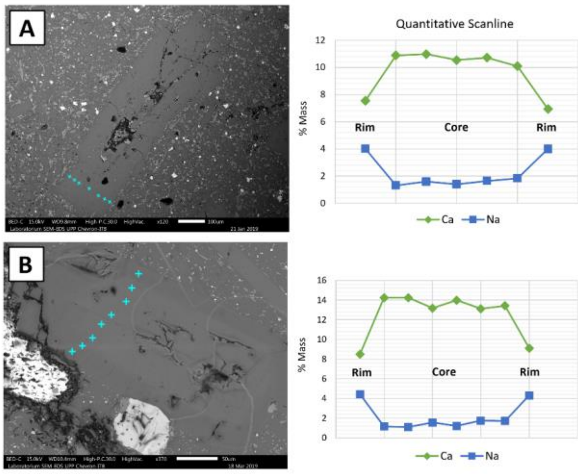

Figure 5. The selected electron images of minerals were identified using SEM-EDS and quantitative scanline. Blue +: approximate analyzed points. (A) Plagioclase in sample GA-TD1 (pre-3200 ± 60 BP period) shows decreasing Ca from core to rim. (B) Plagioclase in sample GA-DA1 (1870 ± 40 – 1040 ± 50 BP) indicates a similar pattern

Pyroxene minerals as phenocrysts (Figure 6A and 6B) occur in subhedral–anhedral forms. Pyroxenes present as local cumulocryst with plagioclase, olivine, and opaque minerals. There are two types of pyroxenes observed in each sample. Orthopyroxene is represented by enstatite, while clinopyroxene has an augite composition (classified from [11]). Based on the scanline test from each eruption period, the mass percentage of Mg in enstatite and augite increases from core to rim (Figure 7A and 7B). Based on geochemical analysis (Figure 7A and 7B), in pre-3200 ± 60 BP period, enstatite has Mg#61–77, whereas augite has Mg#73–78. In the following period, the Mg# content in enstatite increased to Mg#65-76, but Mg# in augite decreased to Mg#71–76. In the 1870 ± 40 – 1040 ± 50 BP period, the Mg# composition in enstatite and augite tended to decrease to Mg#65–75 and Mg#72–77 in order. In post-1040 ± 50 BP period, the Mg# content in enstatite and augite tend to increase to Mg#67–72 and Mg#67–81.

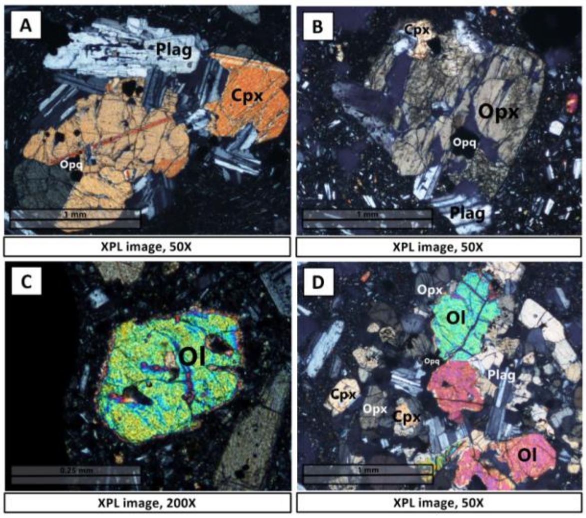

Figure 6. Selected images of minerals during the pre-1963 Mount Agung eruption products are presented from the optical microscope. (A) Clinopyroxene as cumulocryst of Sample GA-TD1 (pre-3200 ± 60 BP). (B) Orthopyroxene in sample BPW-1 (3200 ± 60 – 1870 ± 40 BP BP). (C) Olivine as microfenocryst in sample MTG-5A (1870 ± 40 – 1040 ± 50 BP). (D) Olive, plagioclase, orthopyroxene, clinopyroxene, olivine, and opaque minerals cumulocryst were found in sample MTG-5C (1870 ± 40 – 1040 ± 50 BP). In details, the annotation includes Ol = Olivine, Opq = Opaque Mineral; Cpx = Clinopyroxene; Opx = Orthopyroxene; Plag = Plagioclase

In general, olivine minerals representing the pre-1963 eruption samples occurred as microphenocrysts (Figure 6C). The crystal exhibits subhedral–anhedral forms. Olivine has a reaction rim composed of pigeonite or enstatite (classify using [11]). Based on mineral chemistry analysis (Figure 7C), olivine in pre-3200 ± 60 BP contains Fo62–78 with more Mg-rich core than the rim. In the 3200 ± 60 – 1870 ± 40 BP, the Fo content tends to decrease, becoming Fo60–71, but both core and rim have a wide range of Fo. In the 1870 ± 40 – 1040 ± 50 BP period, the Fo content slightly decreases to Fo59–71. Subsequently, in post-1040 ± 50 BP, the Fo composition increases to Fo66–76. The core seems more enriched with Mg than the rim.

According to scanline tests, the percentage mass of Mg content in olivine decreased in each eruption period. The decreasing content of Mg from the core to the rim (Figure 7C) is caused by the presence of the reaction rim.

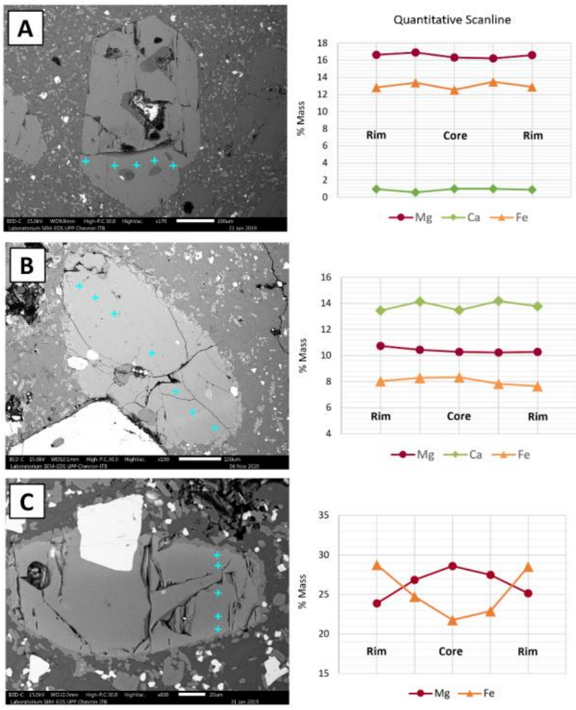

Figure 7. Selected electron images of SEM-EDS and quantitative scanline. Blue +: approximate analyzed points. (A) Enstatite of Sample GA-TD1 (pre-3200 ± 60 BP) generally increases Mg from the core to the rim. (B) Augite in sample DTH-1 (3200 ± 60 – 1870 ± 40 BP) increases Mg from core to rim. (C) Olivine with reaction rim of Sample GA-TU1 (post-1040 ± 50 BP) shows decreasing Mg from core to rim

Opaque minerals are present as phenocrysts with anhedral shapes. Cumulocryst presents locally with plagioclase, pyroxene, and olivine (Figure 6D). Based on the geochemical analysis, the opaque mineral from all eruption periods has a magnetite composition (classified from [12])

Geochemical Analysis

Bulk geochemical analysis was carried out using primary data taken from the published journals by Fontjin [2]. In comparison, this study used data from Dempsey [9] to determine the suitability of clusters distribution. The first analysis is the normative mineral that expresses the molecular proportion [13]. This paper used the CIPW calculation excel sheet program written by Hollocher [14]. Based on Table 2, all samples from each period are characterized by the presence of quartz and hypersthene that shows saturated to highly saturated silica magma.

Next, using plotted data on the Le Bas diagram [15] of total alkali (Na_2O + K_2O) against SiO_2 (Figure 8), the eruption products from each period are as follows: (1) The pre-3200 ± 60 BP consists of basaltic-andesite rocks with SiO_2 53 – 56 wt%; (2) 3200 ± 60 – 1870 ± 40 BP consists of basalt to basaltic-andesite rocks with SiO_2 51 – 56 wt%; (3) 1870 ± 40 – 1040 ± 50 BP consists of basalt to andesite rocks with SiO_2 53 – 58 wt%; (4) The post-1040 ± 50 BP period consists of basaltic-andesite to dacite rocks with SiO_2 53 – 63% wt%.

Magma series or magma affinity can interpret the volcano-tectonic setting [16]. The magma affinity is obtained by plotting the K_2O vs. SiO_2 diagram [17]. The result (Figure 9) shows that all samples are from the calc-alkaline magma series. According to Wilson [16], the plotted samples represent the convergent plate boundaries (subduction).

Table 2. Percentage of normative minerals present in each period of the pre-1963 eruption of Mount Agung. The geochemical data used are from [2]

Eruption Period	**Pre-3200 ± 60 BP**	**3200 ± 60 BP - 1870 ± 40 BP**	**1870 ± 40 BP - 1040 ± 50 BP**	**Post-1040 ± 50 BP**
Deposit Type	Scoria, Pyroclastic Flow	Scoria, Ash Fall	Scoria, Ash Fall, Pyroclastic Flow	Pyroclastic Dlow, Pumice, Scoria, Ash Fall
Normative Mineral (wt%)				
Quartz	2.92 - 6.34	1.35 - 6.92	0.39 - 8.26	2.76 - 15.57
Plagioclase	59.99 - 67.66	56.61 - 72.14	55.35 - 68.3	55.1 - 59.82
Orthoclase	5.73 - 7.45	4.61 - 7.68	4.55 - 11.46	6.68 - 10.7
Corundum	0	0 - 0.64	0	0
Diopside	1.22 - 6.66	0 - 8.36	3.13 - 6.43	0.52 - 8.49
Hypersthene	13.85 - 21.34	13.53 - 24.61	13.66 - 25.49	10.48 - 19.56
Ilmenite	1.44 - 2.07	1.42 - 2.22	1.58 - 2.03	1.12 - 1.73
Magnetite	1.09 - 1.59	1.07 - 1.83	1.15 - 1.59	0.87 - 1.48
Apatite	0.53 - 0.65	0.35 - 0.65	0.37 - 0.65	0.53 - 0.63
Zircon	0.01	0.01	0.01 - 0.03	0.01 - 0.03

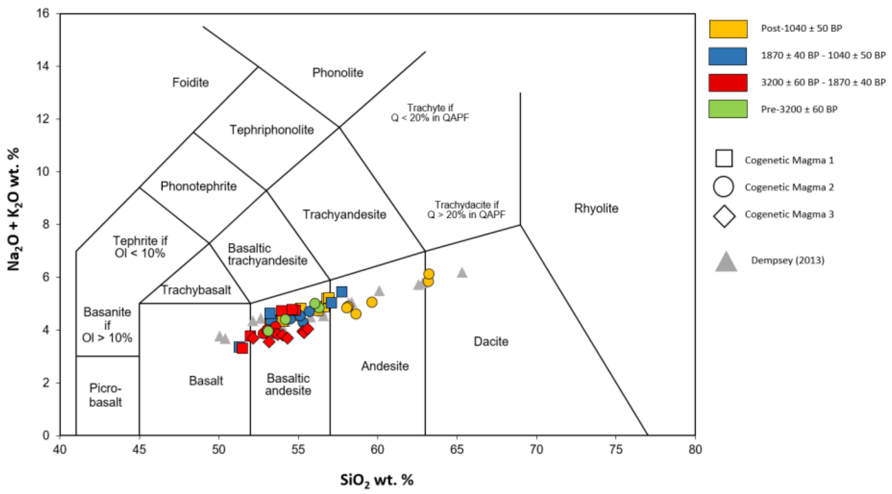

Figure 8. The Fontjin's data [2] was plotted on the Na_2O + K_2O vs. SiO_2 diagram [15] to determine the geochemical rock name. Dempsey's data [9] is used as a comparison

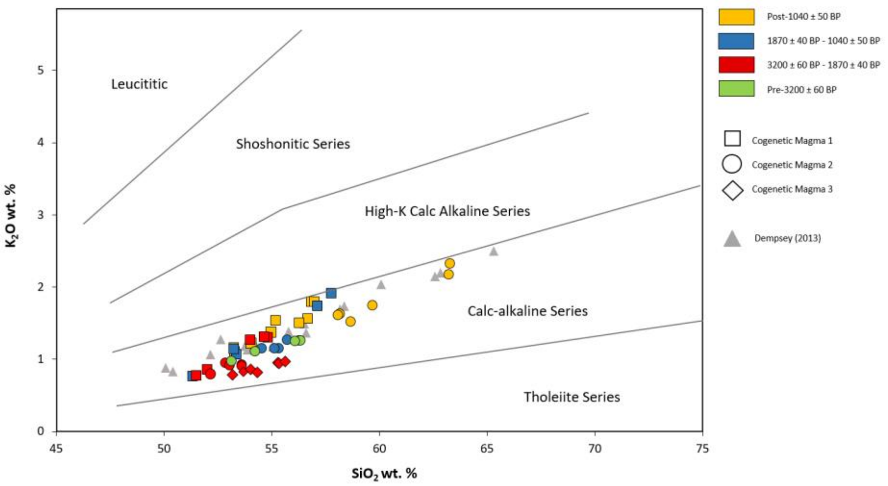

Figure 9. The distribution of Fontjin's data [2] on the K2O vs. SiO2 diagram [17] indicates the magma series of Mount Agung eruption products. Dempsey's data [9] is used as a comparison

Harker diagrams show the change of major elements to SiO2 to define the magmatic activity [18,19]. Crystal fractionation is depicted as a curved pattern. The pattern indicates the depletion of certain compatible elements from the magma melts depending on the mineral phase during crystalization [20]. Harker diagram of TiO2, MgO, Fe2O3, and CaO (Figure 10) shows the occurrence of this process. The older period (pre-1040 ± 50 BP) indicates the fractionation of magnetite, olivine, and pyroxene. Next, the CaO diagram exhibits the plagioclase fractionation, which is predominantly occurred in the younger period (post-1040 ± 50 BP). The differences in the minerals that undergo fractionation are also supported by Dempsey's research [9], which begins from the two fractionation vectors during the magma differentiation process. The evidence is well identified from plagioclase minerals [9,21].

Figure 11 shows data distribution against the two trendlines of plagioclase fractionation [21]. The figure suggests that all pre-1040 ± 50 BP periods lie along the curved line indicating that the plagioclase fractionation was restrained. In contrast, the post-1040 ± 50 BP period follows the other line, which shows the occurrence of plagioclase fractionation. The differences correspond to the previous research that Mount Agung is possibly controlled by a high pressure-deep magma reservoir that can withstand plagioclase fractionation and a shallow magma reservoir with lower pressure [7,9,22].

The tectonic setting was done by plotting trace elements that have been normalized with the primitive mantle onto a spider diagram [23]. Figure 12 suggests that the Rb, Ba, Th, and K (LILE) and La – Sm (LREE) contents are enriched, while Eu – Lu (HREE) experienced a depletion. According to Dirk, these features indicate the properties of a subduction zone [24]. In addition, the Nb content also shows a negative anomaly which is also a characteristic of convergent plate boundaries [16]. Thus, it can be inferred that Mount Agung comes from a volcano associated with a convergent plate boundary (subduction). The types of subduction, island arc or active continental margin, have been distinguished using the ratio of Zr to Zr/Y from Pearce [25].

Based on Figure 13, Mount Agung is produced by the subduction of oceanic crust beneath continental crust. Next, the La/Sm to

IAGI Journal
Volume 1 No. 3, December 2021: 121–136 *e*-ISSN 2776-0111

Th/Nb diagram specifies the differentiation type depending on the tectonic setting [26,27]. Figure 14 shows that in the older period (pre-1040 ± 50 BP), the magma differentiation process is associated with subduction-related enrichment. Meanwhile, in the younger period (post-1040 ± 50 BP), there is a slight influence from the presence of crustal contamination.

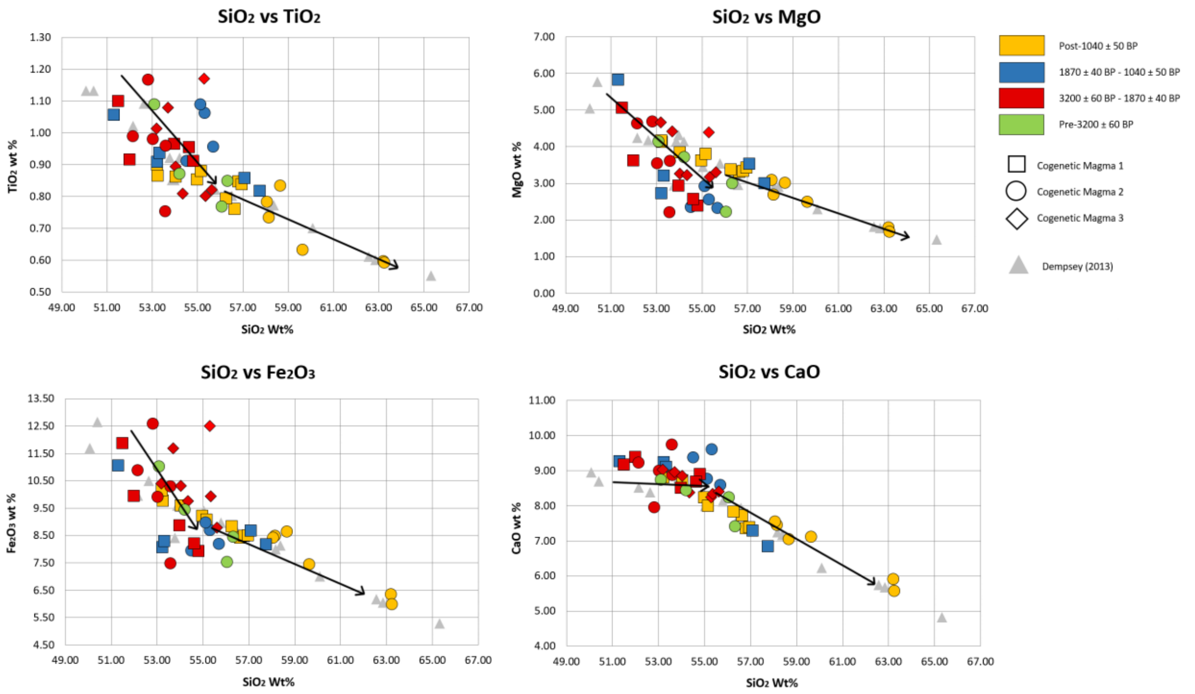

Figure 10. Selected Harker diagrams show the distribution of the major elements SiO2 as a differentiation index. The black arrow indicates the trend of particular minerals depletion. The geochemistry data plotted is from Fontjin [2], while Dempsey's data [9] is used to compare.

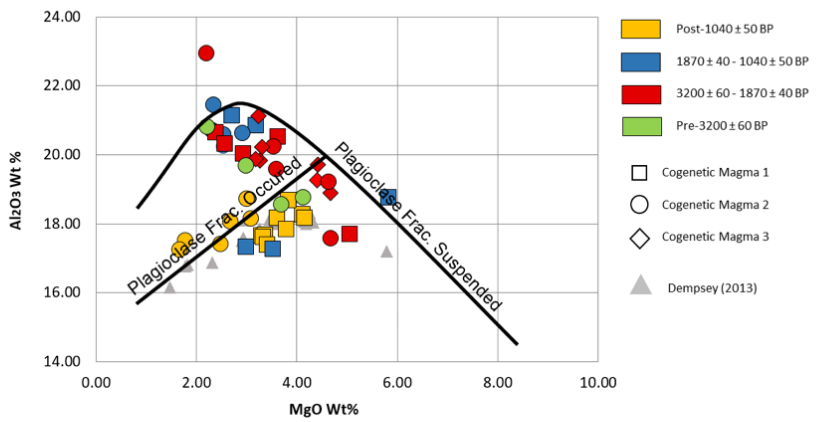

Figure 11. Diagram of MgO against Al2O3 with two trends of plagioclase fractionation [9,21]. The geochemical data used is from Fontjin [2], while Dempsey's data [9] is used to compare

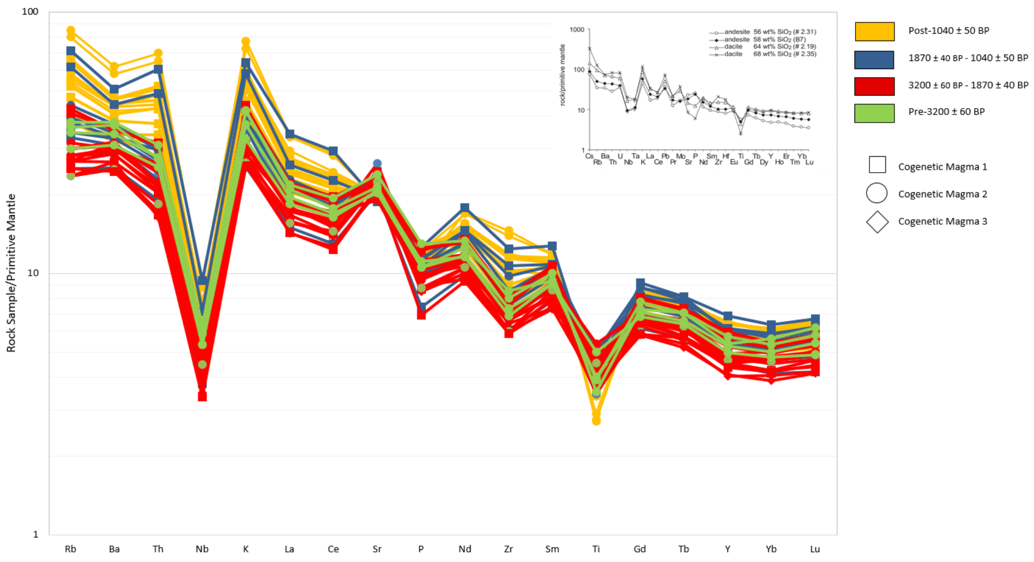

Figure 12. Spider diagram of Mount Agung eruption trace elements. The geochemical data are from Fontjin [2]. The sample was normalized against the primitive mantle [23]. A similar diagram of the Mount Batur eruption products [28] was used to compare.

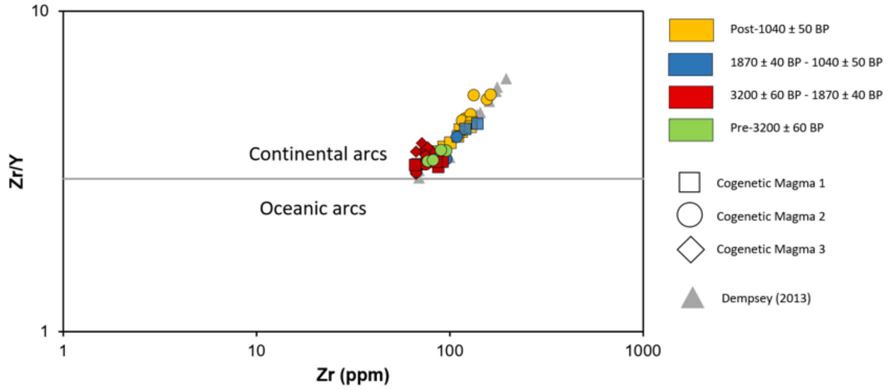

Figure 13. The Diagram of Zr vs. Zr/Y differentiates the continental and oceanic arc [25]. The rock geochemistry data is from Fontjin [2]. Dempsey's data [9] is used as a comparison.

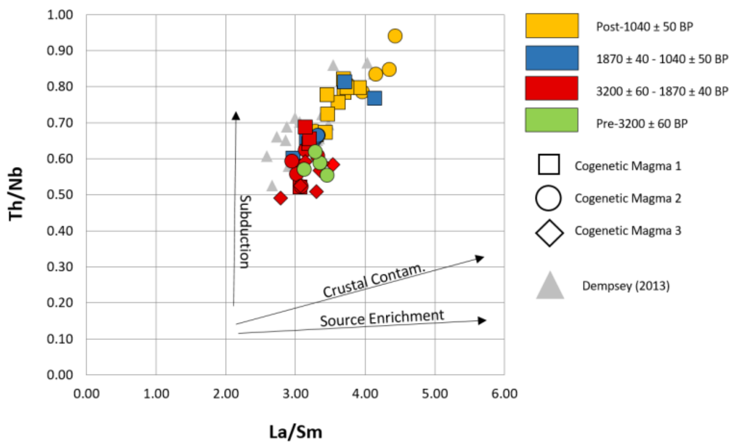

Figure 14. La/Sm vs. Th/Nb diagram with several differentiation vectors [26,27]. The rock geochemistry data is from Fontjin [2]. Dempsey's data [9] is used as a comparison.

DISCUSSIONS

The geochemical analysis reveals a comprehensive result of the Mount Agung magma evolution in the pre-1963. The result was also strengthened by petrography and mineral analysis. Thus, the discussion will compile all the gathered results.

The magma source of Mount Agung is interpreted from the content of Fo in olivine phenocrysts [29]. The original magma from the mantle source exhibits forsterite content for more than Fo88 [16,30]. The Fo content in olivine, representing the pre-1963 eruption, ranges from Fo60–78. This evidences that the primitive magma of Mount Agung is derived from the partial melting process. The SiO_2 content of the primitive magma of Mount Agung can also be interpreted from K_2O against the SiO_2 diagram (Figure 3), assuming that the K2O content is not affected by the crystal fractionation process and can represent the actual content of the magma. According to the diagram, the three trendlines come from one point at lower SiO2. Therefore, it indicates that the three cogenetic magmas are derived from the same magma source. However, if the trendline is extended, the primitive magma has a SiO2 content of ~50 wt%.

Magma evolution began in the pre-3200 ± 60 BP period, which produced basaltic andesite with 53 – 56 wt% SiO2. From the early to the late eruption period, SiO2 content in the rock sample continued to decrease. This indicates a basaltic magma injection. In the 3200 ± 60 – 1870 ± 40 BP period, Mount Agung erupted a basalt to basaltic andesite with SiO2 51 – 56 wt%. The increasing hypersthene as the normative mineral shows that magma saturation has decreased. This period also produced low SiO2 samples. Based on this evidence, the 3200 ± 60 – 1870 ± 40 BP period may become the peak of the basaltic magma injection, which has begun since the previous period. Then, towards the end of the period, the SiO2 content in the rock samples increased, indicating that magma underwent a differentiation process in the form of olivine-pyroxene-magnetite fractionation based on previous analysis. At the beginning of 1870 ± 40 – 1040 ± 50 BP, Mount Agung produced eruptive products with the lowest SiO2 value. It is expected that magma injection has occurred at the beginning of the period and led to the magma mixing with the previously differentiated magma. The eruption period produced basalt to andesite composition with a dominant SiO2 value at 53 – 58 wt%. The percentage of normative quartz increased, suggesting the rise of magma saturation. Subsequently, the magma continued to differentiate. At the beginning of the post-1040 ± 50 BP period, compared to the late period 1870 ± 40 – 1040 ± 50 BP, there was a decrease in SiO2 and K2O values. It indicates that this period started with magma injection first. Mount Agung eruption gradually produced basaltic to dacite andesite rocks with a long interval of SiO2, 53 – 63 wt%. The normative quartz became more abundant while the hypersthene composition decreased. It suggests that magma experienced intensive differentiation during this period. Based on the geochemical analysis, this differentiation is influenced by plagioclase fractionation and a slight presence of crustal contamination, as observed in the geochemical analysis.

The petrographic analysis supports the interpretation of magma evolution. The predominant minerals found are plagioclase, with many types of plagioclase textures. It implies the occurrence of magma evolution [31]. Table 3 shows the presence of plagioclase microtextures in each period. The most abundant textures are coarse sieves, suggesting that magma primarily undergoes a decompression process. The differentiation process occurred simultaneously. The differentiation causes the magma to become saturated with SiO2 that in line with the percentage of shallow-tail and broken crystal textures developed in each period. From the fine sieve and resorption surface, it is suggested that the basaltic magma injection appeared in each period. In the 3200 ± 60 to 1870 ± 40 BP, the abundance of those textures rose compared to the pre-3200 ± 60 BP. It means that magma injection in this period was more intensive. The peak of magma injection occurred at 3200 ± 60 – 1870 ± 40 BP was shown by the coarse sieve microtextures, which were highest during this period. The increase of fine sieve and resorption surface in 1870 ± 40 – 1040 ± 50 BP can be affected by the injection of more basaltic magma, which caused magma to mix with previously differentiated magma. Thus, the dissolution process in plagioclase increases. In the post-1040 ± 50 BP period, fine sieve and resorption surface percentage decreased compared to the previous period. It proves that magma injection was not taking place intensively.

Table 3. The percentage of the plagioclase microtextures represents each pre-163 Mount Agung eruption period.

Eruption Period	Pre-3200 ± 60 BP	3200 ± 60 BP - 1870 ± 40 BP	1870 ± 40 BP - 1040 ± 50 BP	Post-1040 ± 50 BP
Plagioclase Microtexture (%)				
Coarse Sieve	31	29 – 43	14 – 35	27
Glomerocryst	24	10 – 17	7 – 13	31
Fine Sieve	5	0 – 12	0 – 26	6
Resorption Surface	2	3 – 5	0 – 8	-
Fine Oscillatory Zoning	8	4 – 10	5 – 13	6
Rounded Zone	4	0 – 3	0 – 6	-
Synneusis	2	0 – 3	0 – 5	2
Shallow Tail	-	0 – 6	0 – 9	-
Broken Crystal	24	24 – 33	25 – 40	28

The geochemical mineral composition was observed based on the development of %mol forsterite (Fo) in olivine (Figure 15A), %mol of anorthite (An) in plagioclase (Figure 15B), %mol Mg# in enstatite (Figure 15C) and augite (Fig. 15D). The figure above shows that the magma of Mount Agung underwent a differentiation process. In the pre-3200 ± 60 BP period, the erupted magma produced minerals with Fo, Mg#, and An content. Magma injection occurrence during this period was recorded in enstatite and augite, which had an increasing %mass of Mg from the core to the rim. The peak of magma injection occurred in the 3200 ± 60 – 1870 ± 40 BP. This period sequentially produced Agung Lava 5 to 8 (Al 5 – 8), Pawon Lava (Pl), and Pawon Scoria (Psk) units [8]. The peak of magma injection is hypothesized to occur during the formation of the Agung Lava 5 to 6 (Al 5 – 6) units. Afterward, the differentiation process took place and formed the Agung Lava 7 (Al 7), Pawon Lava (Pl), Skoria Pawon (Psk), and Agung Lava 8 (Al 8). From the Fo, Mg#, and An content, the content was decreased in the samples of DTH-1 (representing Al 7) and BPW-2 (representing Pl). The peak of magma injection during the formation of Agung Lava 5 to 6 (Al 5 – 6) units are also supported by the increase of Mg# in enstatite minerals (Figure 15C). Based on the two-phase incongruent melting, if olivine has excess silica, refer to the olivine in the Agung Lava 5 and 6 (Al 5 – 6), enstatite minerals will be formed in the following unit, the Agung Lava 7 (Al 7). This condition is proven by the dominant presence of enstatite in the DTH-1 (representing Al 7). Then in 1870 ± 40 – 1040 ± 50 BP, the %mol

IAGI Journal
Volume 1 No. 3, December 2021: 121–136 *e*-ISSN 2776-0111

of Fo, An, and Mg# tended to decrease. This condition shows that magma continued to undergo a differentiation process. The presence of more basaltic magma injection during this period was recorded in enstatite and augite with the increasing %mass Mg# from the core to the rim. In the post-1040 ± 50 BP, in general, Fo, Mg#, and An increased compared to the previous period. This period is represented by GA-TU1, Agung Lava 12 (Al 12), which formed at the beginning of the period. Based on geochemical interpretation, the beginning of the period is indicated by the injection of basaltic magma, as evidenced by a rise in the content of Fo, Mg#, and An in minerals. Here, the differentiation process takes place. This process can be seen from the scanline results of plagioclase and olivine minerals which show decreasing An and Fo content.

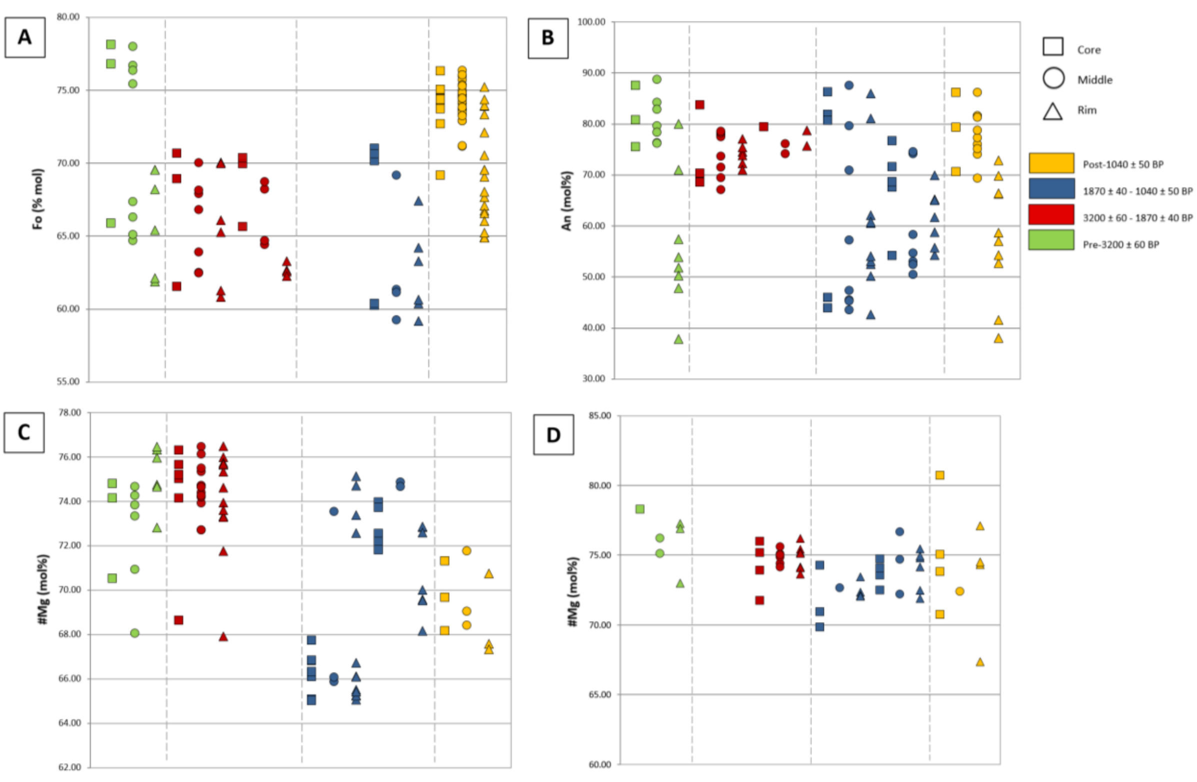

Figure 15. The development of Fo composition in olivine (A), An composition in plagioclase (B), Mg composition in enstatite (C), and Mg composition in augite phenocrysts (D) in each pre-1963 eruption period of Mount Agung.

CONCLUSION

The history of pre-1963 Mount Agung activity began from the partial melting due to the subduction of the convergent plate during the Quaternary Period. The partial melting produced magma with calc-alkali affinity. The primitive magma of Mount Agung probably contains ~50 wt% SiO2. As it rose to the surface, the primitive magma underwent differentiation and was divided into three cogenetic magmas. The magmatic activity of Mount Agung begins in the pre-3200 ± 60 BP period. The eruption of this period resulted in dominant lava units. In this period, the injection of basaltic magma began to occur and reached its peak in the 3200 ± 60 – 1870 ± 40 BP. Then, magma underwent a differentiation process, olivine-pyroxene-magnetite fractionation. This period also produced dominant lava units. At the end of the period, there was an eruption at the Bukit Pawon parasitic cone. In the next period, 1870 ± 40 – 1040 ± 50 BP; the Mount Agung eruption formed large pyroclastic flow units in addition to producing lava units. It denotes that magma continues to differentiate. At the beginning of the period, basaltic magma injection took place, which caused magma to mix with previously differentiated magma. The magma underwent re-differentiation, controlled by the olivine-pyroxene-magnetite fractionation. There was a slight magma injection at the beginning of the post-1040 ± 60 BP. Intensive differentiation process following the subsequent process as evidenced by plagioclase fractionation and probably slight influence from crustal contamination. Eventually, Mount Agung could produce thick pyroclastic fall units, followed by the pyroclastic flow and lava units.

ACKNOWLEDGMENT

This research is part of Penelitian, Pengabdian Masyarakat, dan Inovasi (PPMI) Institut Teknologi Bandung 2021. The fieldwork was partially supported by the USAID’s PEER (Partnership for Enhance Engagement in Research) program with agreement number AID-OAA-A-11-00012.

REFERENCES

1. Kementrian ESDM. Tipe Gunung Api di Indonesia (A, B, dan C) Available online: https://magma.esdm.go.id/v1/edukasi/tipe-gunung-api-di-indonesia-a-b-dan-c#:~:text=Indonesia memiliki jumlah gunungapi aktif,aktif yang dipantau oleh PVMBG (accessed on Nov 26, 2020).
2. Fontijn, K.; Costa, F.; Sutawidjaja, I.; Newhall, C.; Herrin, J. A 5000-year record of multiple highly explosive mafic eruptions from Gunung Agung (Bali, Indonesia): implications for eruption frequency and volcanic hazards. *Bull. Volcanol.* **2015**, *77*, 1–15, doi:10.1007/s00445-015-0943-x.
3. Rampino, M.R.; Self, S. Historic eruptions of Tambora (1815), Krakatau (1883), and Agung (1963), their stratospheric aerosols, and climatic impact. *Quat. Res.* **1982**, *18*, 127–143, doi:10.1016/0033-5894(82)90065-5.
4. Self, S.; Rampino, M.R. The 1963-1964 eruption of Agung volcano (Bali, Indonesia). *Bull. Volcanol.* **2012**, *74*, 1521–1536, doi:10.1007/S00445-012-0615-Z.
5. Zen, M.T.; Hadikusumo, D. Preliminary report on the 1963 eruption of Mt.Agung in Bali (Indonesia). *Bull. Volcanol.* **1964**, *27*, 269–299, doi:10.1007/BF02597526.
6. Tanguy, J.C.; Ribière, C.; Scarth, A.; Tjetjep, W.S. Victims from volcanic eruptions: a revised database. *BVol* **1998**, *60*, 137–144, doi:10.1007/S004450050222.
7. Geiger, H.; Troll, V.R.; Jolis, E.M.; Deegan, F.M.; Harris, C.; Hilton, D.R.; Freda, C. Multi-level magma plumbing at Agung and Batur volcanoes increases risk of hazardous eruptions. *Sci. Rep.* **2018**, *8*, 10547, doi:10.1038/s41598-018-28125-2.
8. Nasution, A.; Haerani, N.; Mulyadi, D.; Hendrasto, M. *Peta Geologi Gunungapi Agung, Bali, Skala 1 : 50.000*; Bandung, 2004;
9. Dempsey, S.R. Geochemistry of volcanic rocks from the Sunda Arc, Durham University, 2013.
10. Williams, H.; Turner, F.J.; Gilbert, C.M. *Petrography : an introduction to the study of rocks in thin sections /*; 2nd ed.; W.H. Freeman: San Fransisco, 1982; ISBN 0716713764.
11. Morimoto, N.; Fabries, J.; Fergusson, A.K.; Guizbourg, I.D.; Ross, M.; Seifert, F.A.; Zussman, J.; Aoki, K.; Gottardi, G. Nomenclature of pyroxenes. *Am. Mineral.* **1988**, *73*, 1123–1133.
12. Buddington, A.F.; Lindsley, D.H. Iron-titanium oxide minerals and synthetic equivalents. *J. Petrol.* **1964**, *5*, 310–357.
13. Kelsey, C.H. Calculation of the CIPW norm. *Mineral. Mag.* **1965**, *34*, 276–282.
14. Hollocher, K. CIPW Norm Calculation Program 2004.
15. Le Bas, M.J.; Le Maitre, R.W.; Streckeisen, A.; Zanettin, B. A Chemical Classification of Volcanic Rocks Based on the Total Alkali-Silica Diagram. *J. Petrol.* **1986**, *27*, 745–750.
16. Wilson, M. *Igneous Petrogenesis*; Springer Netherlands, 1989;
17. Peccerillo, A.; Taylor, S.R. Geochemistry of eocene calc-alkaline volcanic rocks from the Kastamonu area, Northern Turkey. *Contrib. to Mineral. Petrol.* **1976**, *56*, 63–81, doi:10.1007/bf00384745.
18. Harker, A. *The Natural History of Igneous Rocks,*; Methuen & Co.: London, 1909;
19. Winter, J.D. *Principles of Igneous and Metamorphic Petrology*; 2nd ed.; Pearson Education: Harlow, 2014; ISBN 9781292021539.

20. Novak, S.W.; Bacon, C.R.; Peck, D.L. *Pliocene Volcanic Rocks of the Coso Range, Inyo County, California: U. S. Geological Survey Professional Paper 1383*; Denver, CO, 1986;
21. Parman, S.W.; Grove, T.L.; Kelley, K.A.; Plank, T. Along-arc variations in the pre-eruptive H2O contents of mariana arc magmas inferred from fractionation paths. *J. Petrol.* **2011**, *52*, 257–278, doi:10.1093/PETROLOGY/EGQ079.
22. Syahbana, D.K.; Kasbani, K.; Suantika, G.; Prambada, O.; Andreas, A.S.; Saing, U.B.; Kunrat, S.L.; Andreastuti, S.; Martanto, M.; Kriswati, E.; et al. The 2017–19 activity at Mount Agung in Bali (Indonesia): Intense unrest, monitoring, crisis response, evacuation, and eruption. *Sci. Reports 2019 91* **2019**, *9*, 1–17, doi:10.1038/s41598-019-45295-9.
23. Sun, S.S.; McDonough, W.F. Chemical and isotopic systematics of oceanic basalts: Implications for mantle composition and processes. *Geol. Soc. Spec. Publ.* **1989**, *42*, 313–345, doi:10.1144/GSL.SP.1989.042.01.19.
24. Dirk, M.H.J. Petrologi - geokimia batuan Gunung Api Tampomas dan sekitarnya. *J. Geol. Indones.* **2008**, *3*, 23–35, doi:10.17014/IJOG.3.1.23-35.
25. Pearce, J.A. Role of the Sub-Continental Lithosphere in Magma Genesis at Active Continental Margins. In *Continental basalts and mantle xenoliths*; Shiva Publications: Nantwich, Chesire, 1983; pp. 230–249.
26. Plank, T. Constraints from Thorium/Lanthanum on Sediment Recycling at Subduction Zones and the Evolution of the Continents. *J. Petrol.* **2005**, *46*, 921–944, doi:10.1093/PETROLOGY/EGI005.
27. Barresi, T.; Nelson, J.L.; Dostal, J.; Friedman, R. Evolution of the hazelton arc near terrace, british columbia: Stratigraphic, geochronological, and geochemical constraints on a late triassic -early jurassic arc and cu-au porphyry belt. *Can. J. Earth Sci.* **2015**, *52*, 466–494, doi:10.1139/CJES-2014-0155/SUPPL_FILE/CJES-2014-0155SUPPL.XLSX.
28. Reubi, O.; Nicholls, I.A. Structure and Dynamics of a Silicic Magmatic System Associated with Caldera-Forming Eruptions at Batur Volcanic Field, Bali, Indonesia. *J. Petrol.* **2005**, *46*, 1367–1391, doi:10.1093/PETROLOGY/EGI019.
29. Rogkala, A.; Petrounias, P.; Tsikouras, B.; Giannakopoulou, P.P.; Hatzipanagiotou, K. Mineralogical Evidence for Partial Melting and Melt-Rock Interaction Processes in the Mantle Peridotites of Edessa Ophiolite (North Greece). *Miner. 2019, Vol. 9, Page 120* **2019**, *9*, 120, doi:10.3390/MIN9020120.
30. Arai, S. Characterization of spinel peridotites by olivine-spinel compositional relationships: Review and interpretation. *Chem. Geol.* **1994**, *113*, 191–204, doi:10.1016/0009-2541(94)90066-3.
31. Renjith, M.L. Micro-textures in plagioclase from 1994-1995 eruption, Barren Island Volcano: Evidence of dynamic magma plumbing system in the Andaman subduction zone. *Geosci. Front.* **2014**, *5*, 113–126, doi:10.1016/j.gsf.2013.03.006.